

OSCILLATIONS IN FINITE QUANTUM SYSTEMS

G. F. BERTSCH

National Superconducting Cyclotron Laboratory, Michigan State University

R. A. BROGLIA

Dipartimento di Fisica, Università di Milano and INFN Sez. Milano,
and The Niels Bohr Institute, University of Copenhagen



Published by the Press Syndicate of the University of Cambridge
The Pitt Building, Trumpington Street, Cambridge CB2 1RP
40 West 20th Street, New York, NY 10011-4211, USA
10 Stamford Road, Oakleigh, Melbourne 3166, Australia

© Cambridge University Press 1994

First published 1994

Printed in Great Britain at the University Press, Cambridge

A catalogue record for this book is available from the British Library

Library of Congress cataloguing in publication data

Bertsch, George F.

Oscillations in finite Quantum systems / G.F. Bertsch, R.A. Broglia.

p. cm. – (Cambridge monographs on mathematical physics)

Includes bibliographical references and index.

ISBN 0 521 41148 3

1. Many-body problem. 2. Oscillations. 3. Atoms. 4. Metal
crystals. 5. Nuclear physics. 6. Mathematical physics.

I. Broglia, R.A. II. Title. III. Series.

QC174.17.P7B458 1994

530.1'44–dc20 92-40596 CIP

ISBN 0 521 41148 3 hardback

Contents

	<i>Preface</i>	<i>page xi</i>
1	Introduction	1
1.1	Probing the system with photons	2
1.2	A second probe of resonances: inelastic scattering	10
1.3	Energy transfer in inelastic scattering	15
1.4	Inelastic scattering with strongly interacting projectiles	19
1.5	Spin excitations	25
1.6	Excitation by heavy ions	28
2	Basic concepts	33
2.1	Vibrations of continuous systems	33
2.2	Resonance formulas	43
3	Theoretical tools	46
3.1	Operators	46
3.2	Sum rules	49
3.3	TRK sum rule and the oscillator strength	53
3.4	Photon cross section	53
3.5	Spin sum rules	58
3.6	Polarizability sum	58
4	RPA	63
4.1	Linear response	64
4.2	Matrix formulation of RPA	69
4.3	Sum rules	73
4.4	Separable interactions	74
5	Dipole oscillations	81
5.1	Dipole oscillations of electrons and the Mie theory	81
5.2	Nuclei	90

6	Surface modes	99
6.1	Liquid drop vibrations	102
6.2	Surface oscillations of Fermi liquids	106
6.3	Nuclear quadrupole modes	109
6.4	Low frequency vibrations	119
6.5	Higher multiplicities	124
7	Compressional modes	127
7.1	Nuclear breathing mode: classical	128
7.2	Nuclear breathing mode: RPA	130
7.3	Electronic breathing mode	135
8	Spin modes	137
8.1	Isobaric analog resonance	138
8.2	Magnetic modes in nuclei	140
8.3	Gamow–Teller resonances in nuclei	142
8.4	Spin in metal clusters	146
9	Line broadening and the decay of oscillations	148
9.1	Particle escape width	150
9.2	Landau damping	154
9.3	Deformation effects	161
9.4	Optical model of configurational damping	164
9.5	Other internal degrees of freedom	167
10	Thermal effects	171
10.1	Thermal line shifts	175
10.2	Thermal line broadening	176
10.3	A general theory	181
	Appendix A: Mean field theory	187
	Appendix B: Specification of deformations	193
	Appendix C: Finite nucleus compressibility	196
	Appendix D: Nuclear surface reactions	199
	Appendix E: Numerical RPA	203
	<i>References</i>	205
	<i>Index</i>	209

1

Introduction

The behavior of particles interacting under the laws of quantum mechanics is a fundamental concern of both physics and chemistry. The equations describing a system of two particles can be solved efficiently to any needed accuracy. When more than two particles interact simultaneously, however, the *ab initio* quantum mechanical calculations offer little insight.

Fortunately, the actual behavior of the system may be quite simple, even when the underlying equations are not. Depending on the physical situation, only a few degrees of freedom may be relevant. If these degrees of freedom involve the motion of all the particles in the system, we call the motion collective. A familiar example of collective motion is sound in solids. Sound waves are described by a field that acts on all particles in the system in the same way, depending only on the location of the particles. The field is particularly simple for infinite systems because the translational invariance permits only a very regular motion in the normal modes, each mode having a definite wavelength. In finite systems the existence of a surface is very important in determining the normal modes, and the modes cannot be described with definite wavelengths. Nevertheless, we shall see in the finite systems examined here that the important modes are often simple to characterize.

In the language of quantum mechanics, motion in a system is usually described in terms of transitions between energy levels. Each transition has its own frequency, corresponding to the energy difference between the two levels. Collective motion makes its appearance in the quantum language when particular states have large transition amplitudes. We will see that it is then often

possible to describe the transition rather well, even though many of the details of both the initial and final states are not well known.

If we were to make a complete theory of finite systems, we would have to begin with its equilibrium properties. We would first like to know what the stable structure of the system is. How large is it, where are the particles, what is its binding energy? The answers depend not only on the intrinsic forces but upon the conditions under which the system is studied, whether it is cold and in its ground state, or hot and in some statistical ensemble of states.

In this book we pass over these interesting first questions and jump directly to the question, how does the system respond to the external environment? In particular, if the system is subjected to an external field, how do the particles move and how does the system as a whole absorb energy? In classical physics, this is partly answered by finding the normal modes of the system, the small-amplitude vibrations. One of the fascinating properties of the quantum systems is that the classical modes still set the stage for the quantum motion, even though in principle that motion can be much richer.

In this first chapter, we introduce our subject with an overview of the experimental methods used to study the oscillations of finite quantum systems. Later chapters will discuss the theory, starting from classical concepts appropriate to collective motion. We will then build the quantum theory one step at a time.

1.1 Probing the system with photons

Electromagnetic fields provide one of the most important methods for probing many-particle systems ranging from molecules and atomic clusters on the scale of nanometers, down to nuclei on a scale of femtometers. The electromagnetic interaction is completely known, it is strong enough to produce easily observed effects, and yet it is weak enough for the effect of the interaction to be separated from the intrinsic properties of the system under study.

We must first distinguish between static electromagnetic fields and fields that vary in time. With static fields, one studies polarizabilities and static electromagnetic moments, i.e., properties of the equilibrium state. The time-varying fields are generally more interesting, since they can induce internal motion. Physically,

the simplest such field is a free electromagnetic wave, described quantum-mechanically with photons. In the language of photons, one can treat all physical processes using scattering theory. The most important concept is the cross section, which is the probability of the system's absorbing a photon multiplied by the area illuminated by the photon beam. From an experimental side, properties are investigated by measuring the cross sections. A schematic sketch of an experiment to measure a photon cross section is shown in Fig. 1.1. A well-collimated beam of photons passes through a monitor and enters a detector such as a spectrometer. The absorbing material to be investigated is placed in the photon beam between these two instruments, and absorbs some fraction of the beam. The fraction is given by the ratio of photons transmitted, N_f , to photons incident, N_0 . The latter might be determined by taking the absorber out of the beam. The cross section relates the attenuation to the areal density of particles in the cell, n_A . This is given by $n_A = L\rho x/A$, where L is Avogadro's number, ρ is the density of the absorber, x is its length, A the atomic or molecular weight. Then the cross section σ is obtained from

$$\sigma = \frac{1}{n_A} \log_e(N_0/N_f) .$$

This is the attenuation method for measuring cross sections. A simple example of its use is shown in Fig. 1.2. Here is graphed the transmitted intensity of an infrared beam passing through a gas cell containing the molecule HCl. The attenuation factor, I_f/I_0 , is shown as a function of the wavenumber of the photon. Notice that the spectrum consists of a number of narrow lines. These are resonances that correspond to definite transitions between quantum states of the molecule. The HCl molecule is a nearly rigid object at these frequencies; only the quantized states of vibration and rotation play a role in the transition frequencies. The widths of the resonances in this spectrum are extrinsic, associated with instrumental resolution and interactions between the molecules. Other extrinsic effects, such as the Doppler shift of the radiation on a moving molecule, can affect the apparent width as well. The intrinsic width of the resonance is an important property of the molecule itself, but is too small to observe under the experimental conditions of Fig. 1.2. In the usual nomenclature, the width Γ is defined as the interval of energy over which the cross section is

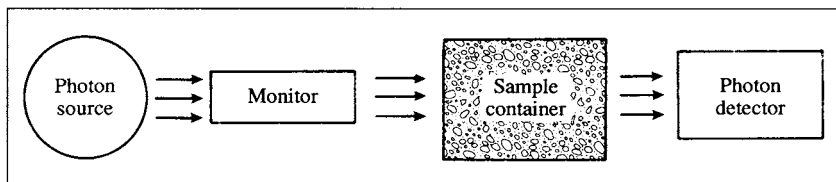


Fig. 1.1. Schematic representation of a photon absorption experiment.

more than half its maximum value. We shall also use the same symbol to express the interval in angular frequency units. The width of a state Γ is related to its mean lifetime τ by the simple formulas

$$\Gamma = \frac{1}{\tau} \text{ (frequency units)}$$

$$\Gamma = \frac{\hbar}{\tau} \text{ (energy units).}$$

In the unit conversion, Planck's constant \hbar is often conveniently expressed as $\hbar = 6.7 \times 10^{-16}$ eV s. Our next example of photon absorption shows a case where the intrinsic width of the excitation is a significant fraction of the photon's frequency. The system studied is the gadolinium atom, and the photons are in the X-ray region. The absorption cross section for photons in the energy range 120–200 eV is shown in Fig. 1.3. The main feature in the spectrum is a broad, somewhat asymmetric peak in the cross section. The resonance is caused by the single-electron transition from an inner d-shell to the valence f-shell in the atom. The width of the peak is intrinsic to the atom and is associated with the lifetime of an electron to escape from the f-shell. In this atom, there is a small barrier in the f-wave potential that produces a resonant state having a finite width.

In the above examples of a molecule and an atom, the spectra are rather directly related to the single-electron atomic shell physics or to the geometric properties of a quantum vibrator. The next example is from systems of atoms that display more subtle interaction effects between the electrons, namely, metal atom clusters. These clusters have been studied intensively recently (cf. the proceedings of the Konstanz conference (1991) and references therein). In typical experiments the clusters are formed in beams and probed with photons or external perturbations while

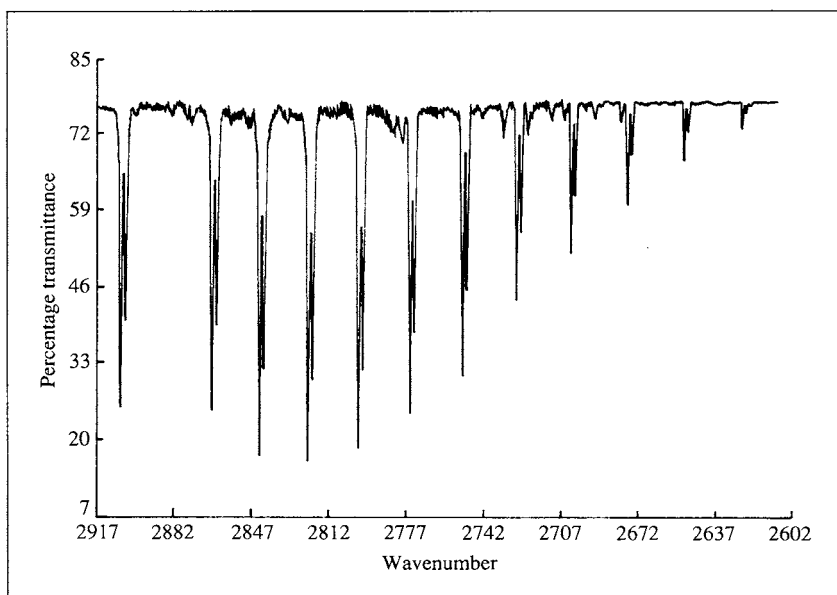


Fig. 1.2. Transmitted intensity of an infrared beam passing through a cell containing gaseous HCl, as a function of photon wavenumber (courtesy of R.A. Bertsch). The lines form a band corresponding to the angular momentum states of the lowest vibrational transition. Wavenumber units n are related to photon wavelength λ and photon energy e_p by $n = 1/\lambda = 8067.5(e_p)_{eV} \text{ cm}^{-1}$.

still in the beam. These stringent conditions are needed to study the clusters because they are generally quite fragile and would disappear on contact with a surface or collision with another particle. The photon absorption spectra for the alkali metal cluster Na_8 is shown in Fig. 1.4. In this system, there is a single prominent peak in the spectral region associated with the valence electron shells. We shall see in Chap. 5 that the strength of this peak is close to the maximum permitted for a valence transition at this energy; its strength nearly exhausts an energy-weighted sum rule. This implies that the valence electrons from all of the atoms participate together in the resonance. The position of the resonance is different from the single-electron shell energy: in a sodium atom, the valence s to p transition has a wavelength of 589 nm, but in the cluster formed by eight atoms the peak is around 500 nm. The collective interaction effects have shifted the peak downward in wavelength and upward in frequency. If this were a classical sys-

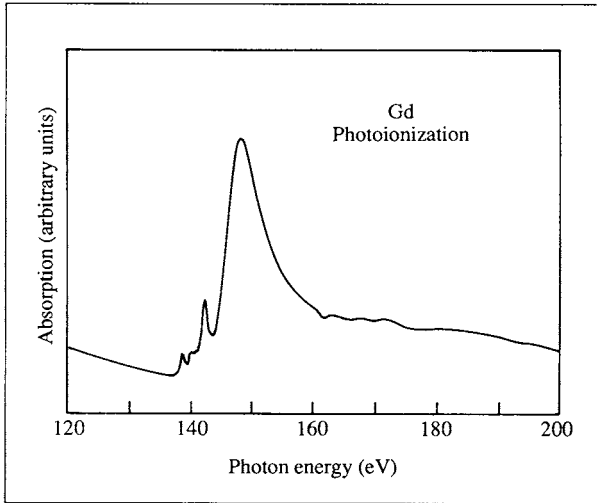


Fig. 1.3. The absorption spectrum of Gd vapor in the range of the transition $4d \rightarrow f$ making use of the 500 MeV synchrotron of Bonn (from Connerade and Pantelouris (1984)).

tem of free electrons, the resonance frequency would be calculable with Newtonian mechanics and electrostatics. The classical theory produces a definite formula, and the corresponding resonance is called the Mie resonance, named after a pioneer investigator of electromagnetic resonances in spherical dielectrics (Mie 1908). In this mode, the electrons simply move back and forth uniformly with a spherical volume, as depicted in Fig. 1.5. In the sodium example, the Mie resonance corresponds to a wavelength of 430 nm, which is smaller than observed. Thus, the finite system behaves somewhere between the limiting extremes of the isolated atom and of a sphere of metallic sodium.

Nuclear physics provides many examples of excitations in which the neutrons and protons making up the nucleus move collectively. For nuclear physics, the convenient length scale is the femtometer, $1 \text{ fm} = 10^{-15} \text{ m}$, and the corresponding energy scale is MeV, megaelectron volts. Photon absorption experiments still follow the classical set-up of Fig. 1.1. The source of photons is most often bremsstrahlung radiation from very energetic electron beams. To select photons of a given energy range, it is not possible to use diffraction as in the case of optical photons or X-rays. Instead, the individual photons must be 'tagged' by measuring simultaneously

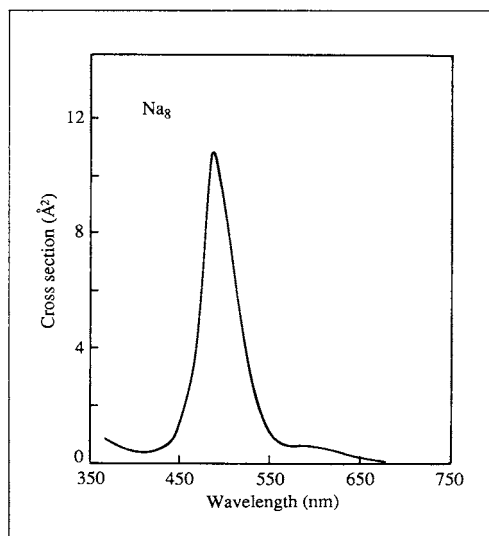


Fig. 1.4. Photoabsorption cross section of Na_8 (in angstroms squared, $1 \text{ \AA} = 10^{-8} \text{ cm}$) as a function of the photon wavelength in nm (Wang et al. (1990)). The clusters were generated by expanding sodium vapor from a high-temperature oven source into a vacuum. The cross section was determined making use of the technique of beam photodepletion. In this method, a pulsed laser beam is directed collinear with but counterpropagating the cluster beam. The beam is detected by ionizing it with another photon source and then accelerating it through a quadrupole mass analyzer. At resonance with the pulsed laser frequency, the cluster beam is depleted due to dissociation of the excited clusters that had absorbed a photon from the laser beam. Note that this experiment measures only the dissociation cross section, which is equal to the absorption cross section only if the cluster has adequate time to decay and nondissociative decay processes are negligible.

the electron that produced the photon and the electron's energy loss. Another difficulty is that the attenuation method for measuring cross sections is less easy to use because only a fraction of the photons are absorbed directly by the nucleus. Most of the beam attenuation comes from interactions with electrons. Nevertheless the attenuation method can be applied, yielding cross sections such as shown in Fig. 1.6. Here we see the photon absorption cross section on the nucleus ^{12}C , measured for photons in the energy range of 15 to 100 MeV. The main feature of the spectrum is a single peak, which is located at an energy near 25 MeV. This is called the giant

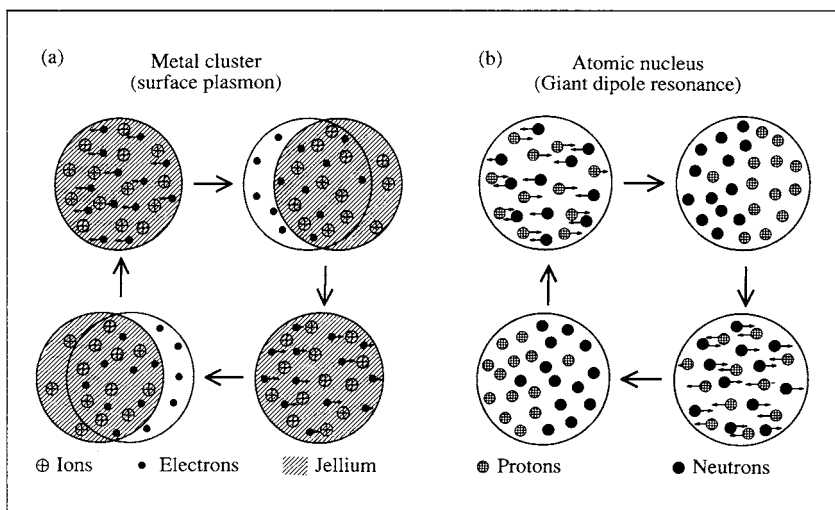


Fig. 1.5. Schematic representation of the giant dipole resonance in atomic nuclei and of the surface plasmon resonance in small metal clusters. The wavelength of the photon exciting these vibrations is large with respect to the diameter of the system. As a result the electric field associated with a passing gamma ray is nearly uniform across the system. In the case of the excitation of the atomic nucleus, the field exerts a force on the positively charged protons, thus separating them from the neutrons. In fact, the neutrons act as having an (effective) negative charge, which oscillates out of phase with respect to the positively charged protons. This is the reason why the giant dipole vibration is an isovector vibration. In the case of metal clusters, the electric field associated with the photon exerts a force on the positively charged ions and an identical force but with opposite direction on the electrons. Because the ions have a mass which is three orders of magnitude larger than that of the electron, the displacement of the electron cloud is much larger than that of the positive background.

dipole resonance. Its strength, as measured by the energy-weighted sum rule, shows that it is a collective excitation involving all of the protons and neutrons. The motion is very similar to that of the Mie resonance. The protons move uniformly back and forth, as shown in Fig. 1.5. The neutrons also move, in an opposite sense from the protons, because, for an internal excitation, the center of mass of the system cannot oscillate, but only recoil. A magnified view of the ^{12}C giant dipole resonance is shown in Fig. 1.7. In this experiment, the cross section for producing neutrons from the

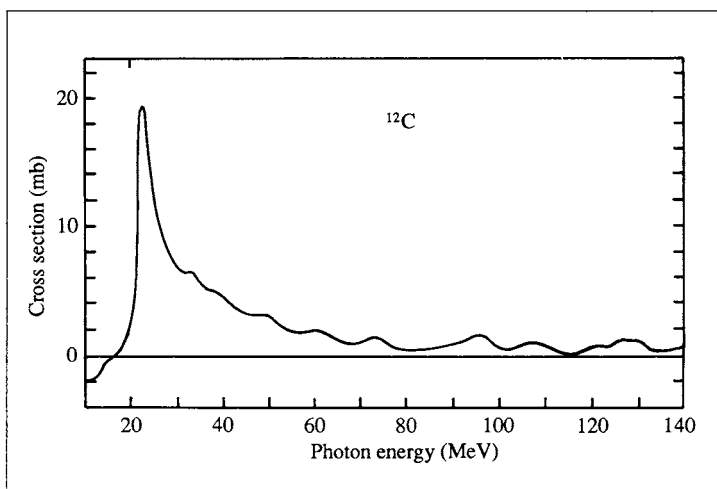


Fig. 1.6. Nuclear photoabsorption cross section of the carbon nucleus, shown as a function of the photon energy. The cross section is given in millibarns ($1 \text{ bn} = 10^{-24} \text{ cm}^2$, $1 \text{ mb} = 10^{-27} \text{ cm}^2$). The peak at around 23 MeV is due to the giant dipole resonance. The angular frequency of the oscillation is given by $\omega = E/\hbar = (23 \text{ MeV})/(6.7 \times 10^{-22} \text{ MeV s}) = 3 \times 10^{21} \text{ s}^{-1}$, corresponding to an ordinary frequency of $f = \omega/2\pi = 5 \times 10^{20} \text{ Hz}$. The data is from Ahrens et al. (1972).

absorbed photons was measured. In contrast, in an attenuation experiment, one measures the total cross section for any beam interaction. The finite width of the resonance is clearly seen, as well as the fact that it is not a smooth function. As we shall see in Chap. 9, in these nuclear systems the width is not due primarily to the escape of particles. It is caused by mixing the collective mode with more complicated internal excitations. The irregularities in these internal states produce the extra structure in this cross section.

It is amusing to look at photon interactions on an even smaller scale, for example, the absorption on a single proton. The experimental spectrum is shown in Fig. 1.8. It shows a resonant peaking similar to that seen for nuclei or larger systems. In this case, the proton behaves as a composite system, and the particles responsible for the resonance are its quark constituents. Although we presented this figure, it is really beyond the domain of our book; the theory is far from adequately developed for quarks and their interactions.

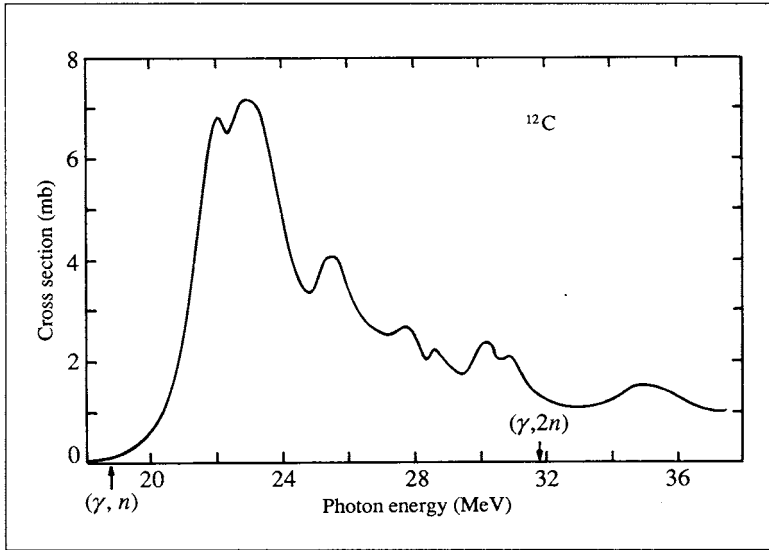


Fig. 1.7. Total photoneutron cross section $(\gamma, \text{total}) = [(\gamma, n) + (\gamma, 2n) + \dots]$ associated with ^{12}C . The photons in this experiment were produced by an electron beam, and their energy measured (“tagged”) by detecting the slowed electrons. The beam passed through a target of ^{12}C , and neutrons produced by the photoabsorption were detected in coincidence with the tagged photons. The giant dipole resonance at 23 MeV is seen in this higher resolution experiment to have a substructure of smaller peaks. The data is from Berman and Fultz (1975).

1.2 A second probe of resonances: inelastic scattering

Resonant photon absorption, which we surveyed in the last section, involves mainly photons whose wavelengths are much larger than the size of the cluster. In the long wavelength limit the electric field is nearly uniform over the entire cluster, and the preferred induced motion is just a uniform displacement of the charges. If we wish to study more complex patterns of motion, the external field must have some spatial variation. Also, fields other than the electromagnetic may be interesting to study in their own right. Such fields can be made by scattering a particle from the system. Indeed, one of the early experiments in quantum mechanics was the famous Franck–Hertz experiment, which produced excitations in atoms by the inelastic scattering of electrons. Of course, that

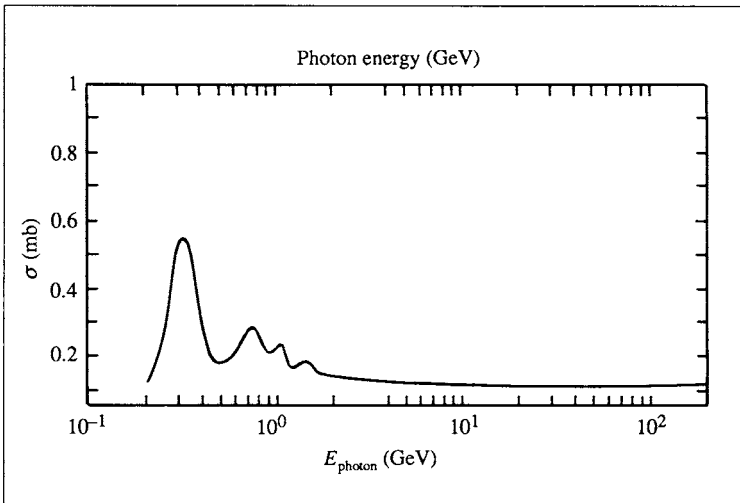


Fig. 1.8. Cross section for photons scattering from protons, shown as a function of the energy of the photon. The strong peak is due to the Δ -resonance, an excited state of the proton (from Hernandez et al. (1990)).

experiment was very crude; the energy transfer to the atom was detected by a decreased current from the slowed electrons.

In modern experiments one measures both the energy loss of the scattered particle and its angular deflection. The energy loss corresponds to the frequency of the excitation in the system as in the photon absorption process, but the angular deflection provides completely new information about the system. The deflection caused by the diffraction of the quantum mechanical waves associated with the particle is related to the spatial distribution of the field acting on the particle. This is a familiar technique for studying bulk materials; the distribution of atoms in a crystal is inferred from X-ray or neutron diffraction patterns.

According to the laws of quantum mechanics, the field produced by a scattering particle has a spatial variation given by the product of the initial and final wave functions of the particle. A mode will be more or less difficult to excite depending on how the motion of the particles in the mode fits together with the spatial variation of the field. Since the field can be varied by looking at scattering in different directions, more detailed information about the excitation mode can be extracted.

Before surveying the inelastic scattering phenomena, it is useful to orient ourselves with a look at elastic scattering. Fig. 1.9 shows the diffraction pattern for neutron and X-ray diffraction on a crystalline solid. The concentration in sharp peaks is, of course, associated with the long-range order of a bulk crystalline material. When the projectile interacts weakly with the medium, the diffraction is easy to interpret. The two wave functions describing the electron in the initial and final channels, are plane waves $\psi_i = \exp(ip_i r)$ and $\psi_f = \exp(ip_f r)$, where p_i and p_f are the angular wavenumber vectors of the waves, related to the momentum P of the particles by the DeBroglie relation, $P = \hbar p$. The product of the two wave functions is also a plane wave, $\psi_i \psi_f^* = \exp(iq r)$, satisfying

$$q = p_f - p_i.$$

The relationship of these wave vectors to the scattering angle is shown in Fig. 1.10. For elastic scattering, the wavenumber q is expressed in terms of the scattering angle θ by the simple formula

$$q = 2p \sin(\theta/2). \quad (1.1)$$

The amplitude for scattering at the corresponding angle θ is directly proportional to the Fourier component of the potential field felt by the projectile at wavenumber q . In a finite system, the Fourier transform varies smoothly with q and thus the scattering will be a smooth function of angle rather than sharply peaked as in scattering from crystals.

Our first example of diffractive scattering in a finite system is the scattering of electrons from the nucleus ^{208}Pb . The differential cross section is shown in Fig. 1.11 as a function of the scattering angle. The three curves show the cross section for elastic scattering and inelastic scattering to the first and second excited states of the nucleus ^{208}Pb . The bombarding energy of the electrons is 500 MeV, giving them a wavelength corresponding to an angular wavenumber $p = E/\hbar c \sim 2.5 \text{ fm}^{-1}$. The cross section falls off very steeply with scattering angle, reflecting the fact that the Coulomb potential is a smooth function with a steeply falling Fourier transform. However, the angular distribution also shows a mild oscillatory behavior, which is traceable to the finite size of the charge distribution.

It is easy to make a qualitative numerical connection between the size of the nucleus, the wavelength of the electron, and the

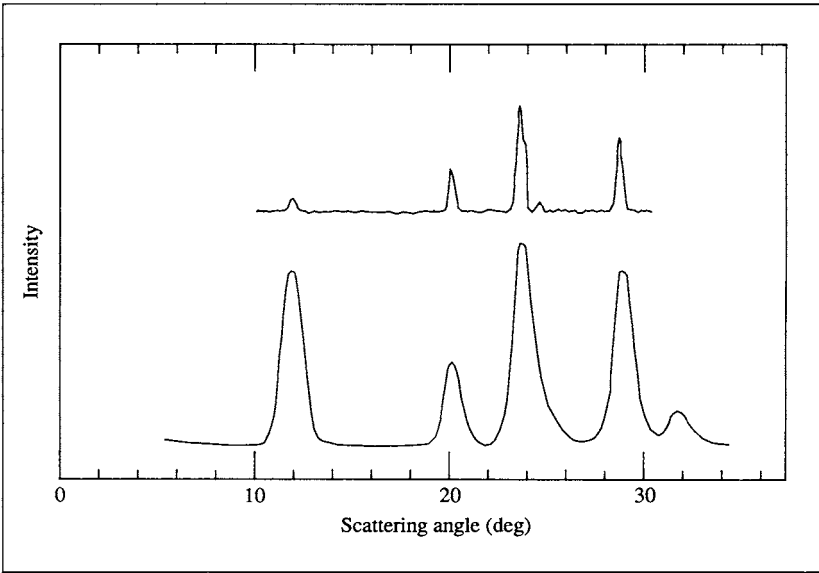


Fig. 1.9. X-ray and neutron diffraction patterns for magnetite at room temperature (from Kittel (1968)).

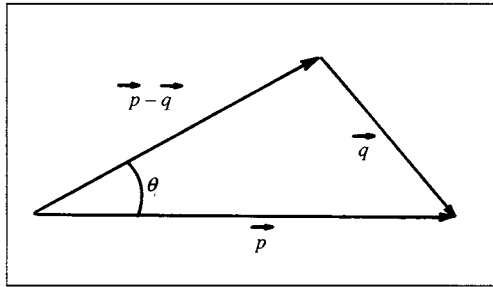


Fig. 1.10. Inelastic scattering of a fast particle with angular wavenumber \vec{p} . Relation between the scattering angle θ and momentum transfer $\hbar\vec{q}$.

period in the diffraction pattern. The observed angular distribution shows an oscillation with successive maxima spaced by about 11° . From eq. (1.1), this corresponds to a change in the angular wavenumber by about $q \sim 0.5 \text{ fm}^{-1}$. An extended object with a well-defined surface at a distance R from the center has an oscillatory Fourier transform whose extrema are approximately separated by an angular wavenumber q satisfying

$$qR \approx \pi. \tag{1.2}$$

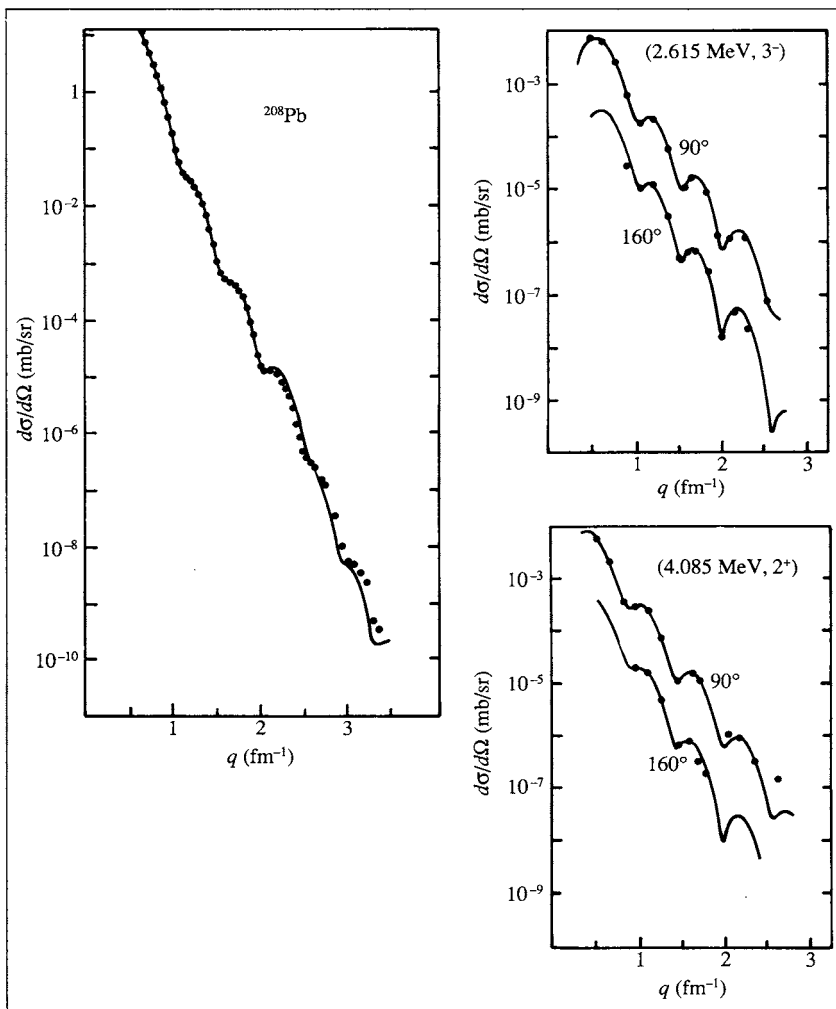


Fig. 1.11. Elastic and inelastic electron scattering differential cross section associated with the ground state, and with the lowest 3^- and 2^+ states of ^{208}Pb , as a function of momentum transfer. The elastic data is from Frois et al. (1977); the inelastic scattering data has been taken from Heisenberg (1981).

This implies, for small angle scattering, that the maxima in the scattering cross section are separated by

$$\Delta\theta = \frac{\pi}{pR}. \quad (1.3)$$

Thus we infer directly from the electron scattering data that the nucleus ^{208}Pb has a radius of about 6.5 fm. This argument is, of course, very rough; the actual theory of the scattering incorporates deviations of the electron wave function from the plane waves, and allows one to infer accurately the complete shape of the charge distribution in the nucleus.

In Fig. 1.12 we show a similar experiment using protons instead of electrons as projectiles. In the region shown, only the nuclear interaction is important. The diffractive structure is more pronounced in this case for two reasons. First, the nuclear interaction is short-range and its Fourier transform does not fall off as rapidly as that of the Coulomb interaction. Second, the projectile is absorbed in the interior of the nucleus, and its wave function cannot be treated as a plane wave any more. The interior absorption, in effect, concentrates the wave physics on the outer part of the nucleus and emphasizes the role of the nuclear surface. Again, the diffraction pattern relates directly to the wavelength of the projectile and the size of the nucleus. The calculation inferring the nuclear size from this data is carried out in the figure caption.

We next give an example of electron scattering from the atomic physics domain. Experiments are usually done with electrons of rather low energy. This makes the experiments more difficult to interpret, because the electron wave functions are strongly distorted. The example is electron scattering on Xe atoms, measured with electrons of 1 eV energy. The angular distribution is shown in Fig. 1.13. This shows a very strong diffraction structure, with a strong maximum at forward scattering angles, a minimum near 30° , and a secondary maximum near 90° . In this example, the bombarding electron has far too low an energy to be treated as a plane wave. The diffractive structure can be understood only in terms of partial wave decomposition of the projectile wave function or detailed numerical models of the potential and the resulting wave function distortion. In any case, if one tries the same estimates as discussed previously, one obtains $q \approx 0.5 \text{ \AA}^{-1}$ and $R \approx 4 \text{ \AA}$, which is somewhat larger than the xenon radius.

1.3 Energy transfer in inelastic scattering

We now examine inelastic scattering more closely from the point of view of the energy transferred to the system. The most detailed

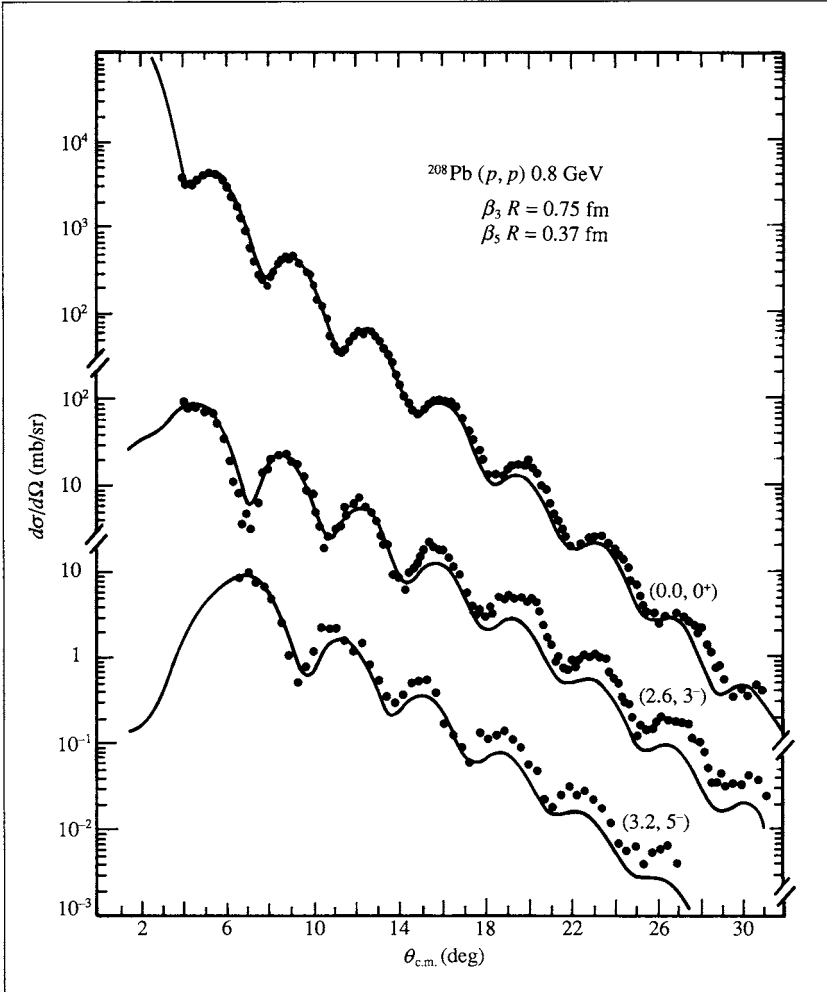


Fig. 1.12. Angular distribution of elastic and inelastic proton scattering for the ^{208}Pb ground state and excited states at 2.6 and 3.2 MeV are given. The data was taken from Blanpied et al. (1978). In this case, the energy of the proton was $E_p = 800$ MeV and its angular wavenumber k is obtained from the relativistic formula $(E_p + m_p c^2)^2 = (m_p c^2)^2 + (\hbar p c)^2$, giving $p = 7.4$ fm $^{-1}$. The diffraction peaks in the data are separated by about 3.5° , consistent with eq. (1.3) for a radius $R \approx 6.8$ fm.

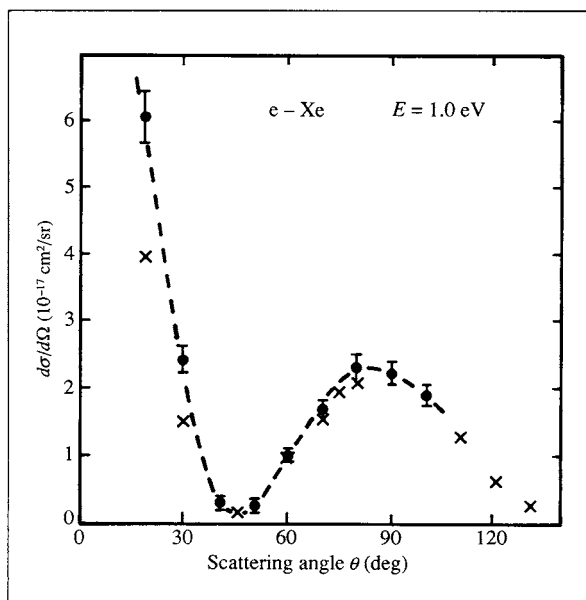


Fig. 1.13. Angular distribution of electrons scattered elastically from xenon at a bombarding energy of 1 eV (from Weyhreter et al. (1988)).

measurements are in nuclear physics, and our examples come mostly from this area. The momentum transfer and associated wave number q are well-defined quantities when we deal with weakly interacting projectiles, and we can discuss the distribution of inelastic scattering as a function of energy loss, keeping the momentum transfer fixed. A schematic energy distribution function is shown in Fig. 1.14. Starting from zero energy loss, we first see a peak associated with elastic scattering. This is shown as Region I in the figure; experimentally the energy resolution would smear the peak over some interval of energy. Going up in energy a little bit, of the order of an MeV, we come to Region II which contains discrete energy levels that can be excited and studied individually. The density of these levels increases very sharply with energy, and at some point individual levels can no longer be resolved. Nevertheless bumps may still be present in the spectrum. One of these is marked as Region III in the figure. This is the region of the giant resonances, which occur at excitations of the order of ten to twenty MeV. They can be excited by inelastic scattering as well as by photon absorption. When the momentum transfer $\hbar q$ is